Lawrence Berkeley National Laboratory
Lawrence Berkeley National Laboratory

Title
Electromigration-induced Plasticity: Texture Correlation and Implications for Reliability Assessment

Permalink
https://escholarship.org/uc/item/37n728h5

Author
Budiman, A.S.

Publication Date
2009-05-04

eScholarship.org Powered by the California Digital Library
University of California

Electromigration-induced Plasticity: Texture Correlation and Implications for Reliability Assessment

A.S. Budiman[1,2,*], P.R. Besser[3], C.S. Hau-Riege[3], A. Marathe[3],
Y.-C. Joo[4], N. Tamura[5], J.R. Patel[†1,5], W.D. Nix[1]

[1]*Dept. Of Materials Science & Engineering., Stanford University, Stanford, CA 94305*
[2]*Spansion Inc., Technology Reliability Engineering (TRE), Sunnyvale, CA 94088*
[3]*Advanced Micro Devices, Inc., Sunnyvale, CA*
[4]*Dept. Of Materials Science & Engineering, Seoul National University (SNU)*
[5]*Advanced Light Source (ALS), Lawrence Berkeley National Laboratory (LBNL),Berkeley, CA 94720*

ABSTRACT

Plastic behavior has previously been observed in metallic interconnects undergoing high current density electromigration (EM) loading. In this study of Cu interconnects, using the synchrotron technique of white beam X-ray microdiffraction, we have further found preliminary evidence of a texture correlation. In lines with strong (111) textures, the extent of plastic deformation is found to be relatively large compared to that of weaker textures. We suggest that this strong (111) texture may lead to an extra path of mass transport in addition to the dominant interface diffusion in Cu EM. When this extra mass transport begins to affect the overall transport process, then the effective diffusivity, D_{eff}, of the EM process is expected to deviate from that of interface diffusion only. This would have fundamental implications. We have some preliminary observations that this might be the case, and we report its implications for EM lifetime assessment in this manuscript.

*Corresponding author; email address: AS.Budiman@SPANSION.com

INTRODUCTION

Most interconnect metals are aggregates of crystalline grains. The crystalline lattice of each grain has a characteristic orientation, and a polycrystal is thus characterized by a distribution of orientations – its texture. Texture governs many of the physical, electrical and mechanical properties of polycrystalline materials. In metallic conductor lines in microelectronics integrated circuits, texture has been known to play important roles in the performance and reliability of the conductors, for instance in electromigration (EM).[1]

Recently, an unexpected mode of plastic deformation has been observed in Al[2,3] as well as in Cu[4-6] interconnects during EM stressing. This deformation occurs not in any random direction, but always in a certain direction related to the interconnect geometries. Texture and crystal plasticity have a close, intertwined relationship; textures evolve during plastic deformation, while plastic deformation often depends on crystallographic orientations. Understanding crystal plasticity and how it progresses in interconnect lines during EM therefore might lead us to fundamental insights on the role of texture in EM.

The grains that exhibit plastic deformation were always observed to deform (bend, rotate or polygonize) transverse to the direction of the electron flow in the line, or in other words, across the width of the line.[4-6] It has been further observed, especially in Cu lines,[4,6] that the occurrence of plasticity can be correlated with the availability of a <112> direction in the proximity of the direction of the length of the line (within about 10°).

In the present study, we investigate a different set of Cu lines fabricated by a different manufacturer. This set of Cu lines differs with the previous set[4-6] in a few ways; chief among them is texture. Using the synchrotron technique of white beam X-ray microdiffraction,[7]

developed in Beamline 7.3.3 at the Advanced Light Source, Berkeley Lab, we follow the evolution of plasticity in Cu polycrystals during similar EM experiments. We observe a strong texture dependence and propose a model to explain the prominent observation.

However, as we establish this texture-plasticity correlation, the effect of plasticity on the Cu EM degradation process remains unresolved. Based on the results and preliminary observations of the present study, we propose a model suggesting that the effect of plasticity might be that of a damaging one to the Cu EM degradation process. Thus, these results may suggest the more desirable texture of Cu interconnect lines for EM.

EXPERIMENTAL

The interconnect test structure used in this study is a variation of a BEoL (Back-end-of-line) process for a 65 nm CMOS technology, as shown in Figure 1. In this technology, the dual-damascene Cu fill process includes a standard Ta-based barrier and Cu seed, electroplated Cu fill, post-plating anneal, chemical-mechanical polish and a dielectric cap layer. Two different inter-layer dielectrics (ILD) were integrated with copper: Cu/low-*k* ILD (Low-*k* = CVD carbon-doped oxide) and Cu/hybrid ILD (Hybrid = Cu/low-*k* at the line level and Cu/FTEOS at the via layer). Both ILD materials were studied in order to provide a comparison of the extent of plasticity. The metal two (M2) lines were studied after partial removal of the top dielectric to expose the capped Cu lines (Figure 1(a)). In these EM tests, the current was forced from the wide, upper metal layer (M3) into narrow M2 (called a V2M2 test) or from a wide lower metal

layer (M1) into a narrow M2 (referred to as a V1M2 test). Both structures are designed to force failure in M2 at its critical dimension.

The first set of test structures consists of 200 µm-long lines, approximately 0.2 µm thick, and 0.5 µm wide. Due to limited beam time, typical of synchrotron experiments, only segments of 50 µm length at both cathode and anode ends of the line were studied (Figure 1(a)). The dielectric is carbon-based CVD oxide ("low-*k*" in Figure 1(c)). The second set of interconnect test structures was prepared with dimensions similar to those of the first one, but with the hybrid ILD material (SiO_2-based). The line length is 200 µm, the thickness is approximately 0.25 µm and the width is 0.7 µm. Similarly, only segments of 50µm length at both cathode and anode ends of the line were studied.

The synchrotron technique of scanning white beam X-ray microdiffraction has been described in a complete manner in a previous publication.[7] The experiment was performed on the Beamline 7.3.3. at the Advanced Light Source, Berkeley, CA. The EM test was conducted at 300°C on a via-terminated test structure (Figure 1(b)). Current and voltage were monitored at 10s increments. The sample was scanned by the 0.8 x 0.8 µm spot-sized white X-ray beam in 0.5 µm steps and a Laue pattern was collected at each step using a MAR CCD detector. A complete set of CCD frames takes about 6 to 7 hours to collect. The exposure time was 20s plus about 6s of electronic readout time for each frame. Laue patterns were subsequently analyzed using the XMAS (X-ray Microdiffraction Analysis Software) to obtain information regarding plastic deformation for each crystal grain in the sample. The current was ramped up to 2 mA (j = 2 MA/cm^2) and then set at that value for the rest of the test (up to 36 hours). The ambient temperature in the synchrotron end-station (hutch) where the tests were performed is 20°C.

RESULTS

The *in situ* electromigration (EM) observations will be described first. Figures 2(a)-(c) show the typical evolution of the Laue diffraction spots during the *in situ* EM test. Figure 2 is early in the EM test, sampled after 36 hours of testing. The observed broadening of the Laue diffraction spots (streaking) represents plastic deformation of the Cu grains induced by EM.[2-4]

As the EM test progresses, plasticity is observed in the Cu grains throughout the line, such as demonstrated in Figure 3(a). Plasticity here may manifest itself either in the form of diffraction spot broadening (streaking) or in the form of diffraction spot splitting (into two or even more different spots). The broadening of the diffraction spots represents crystal bending of the Cu grains in the line, whereas the split diffraction spots indicate the formation of low-angle boundaries or sub-grain structures.[2-4] From the amount of broadening, the bending of the Cu crystal can be calculated. From the degree of splitting, the angle of misorientation between subgrains can be determined.[2-4]

Not only was plasticity observed, but also the direction of the plastic deformation is generally consistent across grains throughout the segments of the line under observation, as shown in Figure 3(a). This is consistent with our observation on the previous set of Cu lines.[4-6] Cu grains plastically deform in a direction transverse to the electron flow direction in the line. Such directionality can simply be accommodated by a distribution of same-sign edge dislocations with cores as illustrated in Figure 3(b), i.e. with the <112> line direction of the dislocations all lining up along the direction of electron flow in the line.

Exact grain orientation mapping of these Cu lines unfortunately could not be obtained in the present study. The X-ray spot size (0.8 x 0.8 μm) currently used in ALS beamline 7.3.3 was

relatively large for the dimensions of these state-of-the-art interconnect lines. That makes diffraction spot indexation very difficult and thus mapping of grain orientations and other further quantitative analyses unreliable. The few Cu grains that we show in Figure 3 were among the limited number of grains in the two Cu lines for which indexation of the diffraction spots happens to be sufficiently clear and unambiguous for this analysis. In general, the larger the Cu grains and the more bamboo-like they are, the more they diffract sharply and give numerous diffraction spots, thus giving higher confidence on the reliability of these results. That being said, it is fortunate that the evolution of Cu diffraction spots before and after some period of EM testing can still be compared qualitatively, as demonstrated in Figure 2.

The extent of the EM-induced plasticity observed in the present samples will now be determined. Figures 4(a) and (b) show still different additional diffraction spots observed during this experiment (after EM testing of 36 hours, at 300 ºC and 2 MA/cm^2 current loading) from Cu lines with the low-k and the hybrid dielectrics, respectively. The diffraction spots have been converted to χ-θ angular space, with χ running along the direction of the length of the line, and θ across the direction of the width of the line.

The observed broadening and spot splitting can be used to obtain information about the dislocation structure induced into the grain by EM. For instance, from the streak length of Figure 4(a), as measured in the digital camera image, and knowing the sample-to-detector distance, we determine the curvature angle of the grain to be 9.8º. Assuming a near bamboo structure, the grain width is the same as the width of the line (0.5 µm), from which we determine the radius of curvature of the grain, R = 2.34 µm. The geometrically necessary dislocation density needed to account for the observed curvature can be calculated from the Cahn-Nye relationship,[8-9] $\rho = 1/Rb$ where b is the Burgers vector. The geometrically necessary dislocation (GND) density is then ρ =

$1.68 \times 10^{15}/m^2$. The total number of dislocations in the area of the cross-section of the Cu line/grain is approximately 142.

To obtain quantitative information on polygonization walls (subgrain boundaries) from the spot split in Figure 4(b) we observe that the Laue spot splitting, $\Delta_\theta = 9.1°$. From this misorientation and Burgers' model of a small-angle grain boundary, $\Delta_\theta = b/L$, where L = dislocation spacing, we find that $L = 16$ Å which amounts to a total of 110 dislocations in the subgrain boundaries in the cross-section of the Cu line/grain. This translates to a GND density of $\rho = 1.12 \times 10^{15}/m^2$.

The extent of the plasticity as described here ($\rho \sim 10^{15}/m^2$) is observed across all grains throughout the segments of both lines with different dielectric schemes. The significance of the difference in our analysis above, in terms of the extent of the plasticity, as well as, its manifestation (grain bending vs. polygonization) between the two Cu lines with different dielectric schemes requires added confirmation. Nevertheless they provide a general indication of the extent of plasticity in these Cu lines.

DISCUSSION

Electromigration-induced Plasticity: The Texture Correlation

Compared to the typical observation of the extent of the EM-induced plasticity in the previous set of Cu interconnect lines,[4-6] this set of samples exhibits at least a two-order of magnitude difference, in terms of GND density (Figure 5). The samples studied previously (referred to as "Samples A") exhibited $\rho \sim 10^{12}\text{-}10^{13}/\text{m}^2$, and the samples in the current study (referred to as "Samples B") exhibited $\rho \sim 10^{15}/\text{m}^2$. Samples A and B differ fairly significantly in dimensions, as well as the dielectric materials used, as shown in Figure 5 (the dimensions are to scale).

Figure 5 shows the typical evolution of the Laue reflections from the Cu lines from the initial state (RT, j = 0, t = time = 0) to the EM state (after some EM, T = 300°C, j ~ 2.0 - 3.1 MA/cm^2, t ~ 36 - 96 hrs). Care was taken in order for the observed intensity contours in the χ-2θ coordinate in Figure 6 to be comparable (the windows all cover areas of squares of a range of 7° - 10° in angle space, and the threshold of the lower-bound intensity display was set to be similar). Thus it is obvious from the relative apparent difference in the extent of streaking/splitting of the Laue diffraction spots that the level of plastic deformation that developed during the course of EM in Samples B is distinctly larger than that of Samples A.

As the two sets of samples (Samples A vs. B) under investigation are provided by different integrated circuit manufacturers, it is not possible to completely quantify the process differences (dielectric type, materials processing and thermal history) in their technologies in this publication. It is known that the two sets of samples differ in terms of dimension and dielectric

materials used; however, it is assumed that the main difference, as far as EM-induced plasticity is concerned, is the crystallographic texture of the Cu lines. From the texture analysis conducted in our previous study,[5] we know that Samples A have a rather weak (111) texture. As mentioned earlier, the exact grain mapping for the present study (Samples B) could not be obtained; however, Samples B came from the same manufacturer of the inlaid Cu lines studied previously.[10] It is therefore reasonable to assert that Samples B would have the typical strong (111) texture as observed by Besser *et al*.[10]

While other process and dimension differences between these two sets of samples include dimensions and dielectric materials are acknowledged, we believe that these differences cannot satisfactorily explain the differences in the extent of plastic deformation. For example, the Cu in Samples A is surrounded completely by dielectric material, which is a fluorinated SiO_2-based dielectric, and thus generally believed to constrain the Cu lines better and should result in less plastic deformation. This is consistent with our observation of Samples A vs. Samples B, but the different dielectric schemes in Samples B, do not appear to affect the level of plasticity in the Cu lines. Another example involves the size effect. Wider lines seem to exhibit more plastic deformation in our previous study,[4-6] such as also shown in Figure 6(a). However, Samples B actually are much narrower, and also much smaller in all cross-sectional dimensions than Samples A, but yet Samples B exhibits two orders of magnitude more EM-induced plasticity.

Figure 6 is a comparison summary of the known information about the Cu lines in Samples A vs. Samples B. First, Samples A shows a weak (111) texture, and we found the extent of EM-induced plasticity in the order of $\rho \sim 10^{12} - 10^{13}/m^2$. Subsequently, Samples B was found with $\rho \sim 10^{15}/m^2$ after similar EM conditions – a significantly larger amount of EM-induced plasticity. Besser *et al.*[10] suggested that Samples B have the typical strong (111) texture. This

observation of significantly larger EM-induced plasticity in Samples B compared to that of Samples A, thus, is consistent with our earlier observation, especially detailed in Reference 6, that the occurrence of plastic deformation in a given grain can be strongly correlated with the availability of a <112> direction of the crystal in the proximity of the direction of the electron flow in the line (within an angle of 10º). In <111> out-of-plane oriented grains in a damascene interconnect scheme, the crystal plane facing the sidewall tends to be a {110} plane, so as to minimize the interfacial energy.[10-12] Therefore, it is deterministic rather than probabilistic that the (111) grains will have a <112> direction nearly parallel to the direction of electron flow or the direction of the length of the line. This is illustrated in Figure 6(b).

In Samples B, most grains are <111> in out-of-plane orientation (such as shown in the FIB mapping in Figure 6(b)), and thus prefer energetically to have the <110> directions normal to the sidewalls, thus causing a <112> direction to be very close to the direction of the electron flow. When this condition is met, our proposed correlation discussed in the previous studies,[4,5] and in greater detail in Reference 6, suggests that plasticity occurs in these Cu grains upon EM, and not only did it occur in the present study, the extent of the plasticity here was rather extreme. Samples A, in the meantime, have only a few grains that are <111> in out-of-plane orientation, which led to the occurrence of plasticity only in these few grains in the Cu lines after EM. In most other grains (i.e. non <111>-oriented grains), a <112> direction of the Cu crystal is not likely to be the direction of the electron flow of the lines. Thus, plasticity was not observed in many grains in the Cu lines of Samples A.

Dislocation Cores as Fast Diffusion Paths in Metallic Interconnects

The observed plasticity described above (see Figure 3) leads to a concentration of same-sign edge dislocations with cores running along the direction of electron flow, as illustrated three-dimensionally in Figure 7. When this configuration of same-sign edge dislocations extends through grains along the full length of the interconnect lines, the dislocation cores can serve as additional paths for diffusion of atoms from one end of the interconnect line to the other. Dislocation cores are, in general, already recognized as fast diffusion paths,[13] but in this configuration especially, their contribution to the overall migration of atoms from the cathode to the anode end of the line is even more pronounced. Furthermore, when the concentration of these dislocations becomes high enough, their contribution to the overall effective diffusivity (D_{eff}) can no longer be neglected.

In this context the effective diffusivity can be written as

$$D_{eff} = \frac{\delta}{h} D_{\text{int}} + \rho a_{core} D_{core}^{eff} \quad , \qquad \text{(Eq. 1)}$$

where a_{core} is the cross-sectional area of dislocation cores, D_{core}^{eff} is the effective core diffusivity, ρ is the dislocation density, and δ, h and D_{int} are the effective interface diffusion thickness, the height of the line and the diffusivity of the interface, respectively. It is necessary here to use D_{core}^{eff}, the effective core diffusivity (instead of simply D_{core}, the core diffusivity), because for the dislocation cores to have an effect on mass flow along the full length of the line, a continuous diffusion path (across grains) must be available for atoms to transport from the cathode end to

the anode end of the lines. Considering the mostly bamboo grain structure that our interconnect lines have (as shown in Figure 3), this requires consideration of grain boundary diffusion, as atoms eventually hit the grain boundaries and have to travel some distance in the grain boundary before finding another set of dislocation cores (belonging to the neighboring grain) to continue their travel to the other end of the line. This is illustrated schematically in Figure 8. Thus, the effective core diffusivity, D_{core}^{eff}, here will be defined as the effective diffusivity along the dislocation cores when the effect of the grain boundary diffusion is taken into account.

It is obvious that only when the effect of the grain boundary diffusion is negligible (or in other words, the grain boundary diffusion is a fast enough process), can dislocation cores provide a competitive alternative diffusion path and influence the overall effective diffusivity, D_{eff}, as suggested in Equation 1. In order to study quantitatively the impact of this grain boundary diffusion on the overall dislocation core diffusion (D_{core}^{eff}), we derive the kinetics for such a model and arrive at the expression below for D_{core}^{eff} (the full derivation is provided in the appendix),

$$D_{core}^{eff} = D_{core}\left\{\frac{2\delta_{gb}D_{gb}L}{2\delta_{gb}D_{gb}L + r_{core}^{2}D_{core}\ln(R/r_{core})}\right\}. \qquad \text{(Eq. 2)}$$

where δ_{gb} and D_{gb} are the effective width and diffusivity of the grain boundary, respectively, L *is the* overall length of the diffusion path, r_{core} is the radius of the dislocation core, and R is the mean distance in the grain boundary diffusion to the next dislocation core.

The influence of grain boundary diffusion on the overall/effective dislocation core diffusivity, D_{core}^{eff}, thus depends on the relative magnitude of the two terms in the denominator in the Equation 2. If

$$2\delta_{gb} D_{gb} L >> r_{core}^2 D_{core} \ln(R/r_{core}) , \qquad \text{(Eq. 3)}$$

then as evident from Equation 2, D_{core}^{eff} degenerates into simply D_{core}, or in other words, there is very little influence of the grain boundary diffusion in the overall scheme in Figure 8. If the reverse is true, D_{core}^{eff} will be much smaller than D_{core}, in which case it is clear that the grain boundary slows down the overall diffusion significantly.

Referring now to the textbook values for grain boundary and core diffusion compiled in Table 1,[14- 17] and compared in Table 2, it is evident that the $2\delta_{gb} D_{gb} L$ term in Equation 2, as well as in Equation 3, is at least 4 orders of magnitudes larger than the $r_{core}^2 D_{core} \ln(R/r_{core})$ term. This leads to the degeneration of D_{core}^{eff} into simply D_{core} in Equation 2, reducing to Equation 4

$$D_{core}^{eff} \approx D_{core} \quad . \qquad \text{(Eq. 4)}$$

The practical implication of Equation 4 is that a practically continuous pipe (dislocation core) diffusion path across multiple grains between the cathode end and the anode end of the line is indeed available for atomic transport in the Cu test structures under accelerated EM testing.

An extreme would be to take the activation energy for grain boundary diffusion, $E_{A,gb,}$ to be the E_A for lattice diffusion, which is 2.04 eV.[14] This is a much higher activation energy than

that of grain boundary diffusion. In this case, we show that the combined diffusivity would be dominated by such slow diffusion in the hypothetical "grain boundary." The effective transport through dislocation cores in this case would be slowed down by nearly 4 orders of magnitude due to the effect of the hypothetical grain boundary. This is shown in Figure 9, which compares calculated diffusivities as a function of temperature for three different schemes of diffusion (D_{core}, D_{core}^{eff} “as it is,” and D_{core}^{eff} “extreme,” as defined above). The D_{core}^{eff} “extreme” line is close to 4 orders magnitude lower than D_{core}^{eff} line (with crosses), which are practically on top of each other with the D_{core} line (with buttons) as suggested by Equation 4.

It is therefore reasonable to propose that a fully continuous network of dislocation cores running along the direction of the length of the line, slowed only by less than 0.01% by grain boundary diffusion, exists in the Cu interconnect lines studied during EM under accelerated test conditions in this study. This makes it a viable alternative for global transport of atoms in Cu interconnects under EM bias.

The existence of a viable path of dislocation core diffusion alone, however, is not sufficient to influence the overall kinetics in Equation 1, that is, if the dislocation density (ρ or ρ_{GND}) is not high enough. We cover this situation below and show the importance of the experimental results of the present study in understanding the overall kinetics in Cu interconnect lines under EM.

Density of Core Dislocations (ρ_{core}): Extent of Plasticity

Diffusion along dislocation cores ("pipe diffusion") has been commonly included in models of diffusion-controlled deformation in bulk materials.[14] Suo[18] considered the motion and multiplication of dislocations under the influence of an electric current in a conductor line, and suggested that EM-driven dislocation multiplication could itself lead to dislocation densities high enough to affect EM degradation processes. Oates,[19] however, did not see any diffusivity effects that could be attributed to dislocations in his experimental study. Baker *et al.*[13] through their experimental study of nanoindented Al lines (width = 1 μm, mean grain size = 1.1 μm) showed that the effect of a dislocation density of $10^{16}/m^2$ is comparable to diffusion through a grain boundary. These studies all essentially suggest that if the dislocation density is sufficiently high, it may affect the overall EM degradation processes in metallic interconnects, and thus could have fundamental implications.

We have, earlier in the manuscript, established that dislocations with cores running along the electron flow direction and densities in the order of $10^{15}/m^2$ are present in the Cu lines undergoing EM (accelerated test conditions) for 36 hours. Figure 10 is a comparison of calculated diffusivities as a function of temperature between the interface diffusion path and those of dislocation cores of various densities in Cu interconnect lines ($10^{12}/m^2$, $10^{15}/m^2$, and $10^{17}/m^2$) when each diffusion mechanism is assumed to act alone. The diffusivities are calculated based on diffusion coefficient values in the literature[14-15] for Cu interconnect lines (tabulated in Table 3), and for the interconnect dimensions as used in the present study.

The dislocation density observed in the present study ($\rho_{GND} = \rho_{core} = 10^{15}/m^2$) is illustrated as the solid line in Figure 10, illustrating that dislocation core diffusion is on the same

order of magnitude as that of interface diffusion (the dotted line) at the test conditions (T = 300ºC or $1000/T$ = 1.75/K). Thus, a core dislocation density of $10^{15}/m^2$ is the dislocation density threshold necessary for dislocation core diffusion to be on par with interface diffusion. In other words, at this dislocation density the contribution of dislocation cores to the overall/effective diffusivity in the Cu line during accelerated EM is expected to be at least the same order of magnitude as interface diffusion and thus cannot be neglected.

It is to be noted, however, that at temperatures at or below 100 ºC, the required dislocation density for cores to have a significant contribution to the diffusion would be on the order of $10^{17}/m^2$ (the dashed line in Figure 10). These lower temperatures correlate with the typical use or operational conditions of the interconnects. The typical initial (as fabricated) dislocation density in Cu/metallic lines was taken to be $10^{12}/m^2$ (following Reference 13), and the corresponding diffusivity is shown by the dashed-dotted line in Figure 10.

It is therefore reasonable to propose that the contribution from the dislocation core diffusion (the second term in Equation 1) can no longer be neglected in the Cu lines now that we have evidence of the existence of such high density of dislocation cores in the real Cu interconnect structure. It is certainly true in the Cu lines investigated in the present study especially during EM at accelerated test conditions. The contribution from dislocation cores would enhance the EM diffusion, or in other words, the total EM flux (J_{EM}), since the total or overall diffusion includes the existing, usually-dominant interface diffusion, plus the observed dislocation core or "pipe" diffusion. The increase in this core diffusion to the point of significance in the overall EM diffusion is related to the kind and the extent of plasticity induced by the EM process itself (i.e. through the increase in the core dislocation density from the pre-EM density $\rho_{core} = 10^{12}/m^2$ to the observed density $\rho_{core} = 10^{15}/m^2$).

The result of this study gave a key piece of experimental evidence that opens up the possibility that such a high dislocation density may generally be present in the Cu test structures undergoing EM. The circumstances and the important implications of this special configuration of dislocation cores for the EM degradation processes warrant discussion, as do the EM reliability assessment methodologies. With ρ_{GND} ~10^{15}/m^2 observed in this study, and D_{core}^{eff} that is not much reduced by grain boundary diffusion (as derived in the appendix), the second term in Equation 1 (ie. the contribution of the dislocation core diffusion) can indeed no longer be neglected. This means it will have important implications to the fundamental understanding of the EM degradation processes, as well as to the electromigration reliability assessment methodologies.

The Extra Dependency on *j* – Implications for EM and Reliability Assessment Methodology

If ρ should increase with j, then we will find that D_{eff} (the overall/effective diffusivity of the EM process) should also increase with j. Consequently, there will be an extra EM flux, and thus an extra reduction in the time to failure of the device with increasing j. This is an extra dependency on j, which would manifest itself in the value of the current density exponent, n (in Black's equation[20]), being >1.

$$MTF = A\left(\frac{1}{j}\right)^n \exp\left(\frac{E_A}{kT}\right) \qquad \text{(Eq. 5)}$$

The fact that n is usually found in real cases to be > 1 (as opposed to $n = 1$ for the prevailing model of void growth limited failure)[21-23] suggests that this extra dependency on j, especially at high temperatures of the test conditions, could be due to dislocation core diffusion. In other words, the higher n could be traced back to the higher level of plasticity in the crystal, and the closer n is to unity, the less plasticity must have influenced the electromigration degradation process.

Kirchheim and Kaeber[24] experimentally observed the *MTF* dependency on current density, j, in an Al conductor line, for a wide range of j, such as shown in Figure 11 (the solid black dots with error bars were the original data points). It clearly shows that at low current densities, the *MTF* data is best fit by $n = 1$ (straight solid line), while at higher current densities, the *MTF* data is better fit by $n > 1$ (curved dotted line). Kirchheim and Kaeber however suggested in their paper that these deviations occurring at higher current densities might have been caused by Joule heating.[24]

Plasticity, especially in the form described in this paper as well as in the literature,[2-6, 25, 26] could just as likely be the source of such deviations of *MTF* dependency on j at high current densities. As j increases, plasticity also increases leading to increasingly higher EM fluxes (the dashed, arrowed lines in Figure 11), and thus increasingly lower *MTF*, and therefore eventually a current density exponent, $n > 1$ has to be used to fit the failure time distribution.

However, under use conditions in which the temperature is much lower (eg. 100°C), the level of ρ associated with such elevated diffusivity is almost impossible to reach, so that this plasticity-amplified diffusivity is associated only with the high temperature and high current density of the accelerated EM test. In other words, there is not likely to be much plasticity under use conditions, and thus the diffusivity is dominated only by interface diffusion, and

consequently the *MTF* dependency on j should follow the $n = 1$ line. This is consistent with the observations of Kirchheim and Kaeber[24] (Figure 11 shows data following $n = 1$ line at low reduced current densities, 0.2 – 1 MA/cm^2). This interpretation of the Kirchheim and Kaeber data is consistent with the physical model (void growth limited failure) which has also been observed through *in situ* electromigration studies by Zschech *et al*.[27] on samples/materials similar to those used in the present study.

It can be further stated that plasticity-amplified diffusivity is simply an extra mode of deformation under test conditions (which is not typically present under use conditions), and that its effect is wholly captured in the n value being greater than unity. This plasticity-inflated n could thus lead to inaccurate extrapolations of lifetimes under use conditions. This is illustrated in Figure 12.

Figure 12 illustrates the danger of overestimating device lifetime if, for example, we simply take the three *MTF* data points under accelerated j (the three solid black triangles in Figure 12), and based on these data points, we calculate n (which will be larger than 1), and then we use this n to extrapolate from the accelerated condition (high j) to the use condition (low j). That extrapolation is shown by the dashed-dotted line in Figure 12, and it clearly is an overestimation of the device's actual lifetime (approximated by the *MTF* data at low reduced current density).

To improve the accuracy of the reliability assessment of devices under use conditions, we propose that the effect of plasticity has to be removed from the EM lifetime equation. This can be done simply by insisting on $n = 1$ in our lifetime assessment (i.e., j_{max} calculation) which in most typical EM test conditions will result in a more conservative prediction of device lifetime, such as illustrated by the dashed line in Figure 12.

CONCLUSIONS

Plastic deformation behavior of Cu polycrystals during electromigration (EM) experiments has been observed using a synchrotron technique involving white-beam X-ray microdiffraction. The occurrence of the plastic behavior observed in these Cu lines appears to depend on the availability of a <112> direction along the length of the Cu lines as the rotation axis of the plastic deformation. Furthermore, with the present set of Cu lines, we found that the extent of the EM-induced plasticity was significantly larger compared to that observed in a previous study. We propose that the crystallographic texture of the Cu lines plays a primary role in controlling the plastic behavior of the interconnect lines. Strong (111) texture leads to high preference of <112> direction along the length of the line, and this subsequently leads to a higher tendency for the grains to behave plastically in response to EM stressing. The extent and configuration of dislocations in the Cu grains induced during this accelerated EM testing could lead to another competing EM diffusion mechanism in addition to interface diffusion. It is suggested that this plasticity effect can be correlated to the measured value of current density exponent, n, in Black's equation and thus has important implications for the way device lifetime/reliability is assessed. A new method of lifetime extrapolation for electromigration (EM) by insisting to use $n = 1$ is proposed that avoids potentially dangerous and overestimating lifetime prediction based on the current methodologies using measured value of n from accelerated test conditions.

ACKNOWLEDGMENTS

The authors would like to thank Advanced Micro Devices (AMD) for generous support and for fabricating the samples in the study. Bryan Tracy of Spansion provided the FIB images in Figure 1. One of the authors (ASB) would like to thank John M. Ennals, the AMD/SRC Program Manager at AMD, for the opportunity of a Summer Internship Program in 2006. Both ASB and WDN gratefully acknowledge support by the U.S. Department of Energy, Office of Basic Energy Sciences through Grant No. DE-FG02-04ER46163. The Advanced Light Source (ALS) is supported by the Director, Office of Science, Office of Basic Energy Sciences, of the U.S. Department of Energy under Contract No. DE-AC02-05CH11231 at the Ernest Orlando Lawrence Berkeley National Laboratory (LBNL).

REFERENCES

1. L. L. Vanasupa, Y. C. Joo, P. R. Besser, and S. Pramanick, *J. Appl. Phys.* **85**, No. 5, 2583, **1999**
2. B. C. Valek, J. C. Bravman, N. Tamura, A. A. MacDowell, R. Celestre, H. Padmore, R. Spolenak, W. L. Brown, B. W. Batterman, and J. R. Patel, "Electromigration-induced Plastic Deformation in Passivated Metal Lines," *Appl. Phys. Lett.*. **81**, p. 4168, **2002**
3. B. C. Valek, N. Tamura, R. Spolenak, W. A. Caldwell, A. MacDowell, R. S. Celestre, H. A. Padmore, J. C. Bravman, B. W. Batterman, W. D. Nix, and J. R. Patel, *J. Appl. Phys.* **94,** 3757, **2003**

4. A. S. Budiman, N. Tamura, B. C. Valek, K. Gadre, J. Maiz, R. Spolenak, W. D. Nix, and J. R. Patel, "Crystal Plasticity in Cu Damascene Interconnect Lines Undergoing Electromigration as Revealed by Synchrotron X-Ray Microdiffraction," *Appl. Phys. Lett.*. **88**, 233515, **2006**
5. Arief S. Budiman, N. Tamura, B. C. Valek, K. Gadre, J. Maiz, R. Spolenak, W. A. Caldwell, W. D. Nix and J. R. Patel. Unexpected Mode of Plastic Deformation in Cu Damascene Lines Undergoing Electromigration, *Mater. Res. Soc. Symp. Proc.*, **812**, **2004**.
6. Arief S. Budiman, N. Tamura, B. C. Valek, K. Gadre, J. Maiz, R. Spolenak, J. R. Patel, and W. D. Nix. Electromigration-Induced Plastic Deformation in Cu Damascene Interconnect Lines as Revealed by Synchrotron X-Ray Microdiffraction, *Mater. Res. Soc. Symp. Proc*., **914**, **2006**
7. N. Tamura, A. A. MacDowell, R. Spolenak, B. C. Valek, J. C. Bravman, W. L. Brown, R. S. Celestre, H. A. Padmore, B. W. Batterman and J. R. Patel, *J. Synchrotron Rad*. **10**, 137-143, **2003**
8. R. W. Cahn, *J. Inst. Met.*, **86**, p. 121, **1949**
9. J. F. Nye, *Acta Metall.*, **1**, p. 153, **1953**
10. P. Besser, E. Zschech, W. Blum, D. Winter, R. Ortega, S. Rose, M. Herrick, M. Gall, S. Thrasher, M. Tiner, B. Baker, G. Braeckelmann, L. Zhao, C. Simpson, C. Capasso, H. Kawasaki, and E. Weitzman, "Microstructural Characterization of Inlaid Copper Interconnect Lines," *J. Elec. Matls*., **30**, No. 4, p. 320, **2001**
11. J.E. Sanchez, Jr. and P.R. Besser, *Proceedings of the International Interconnect Technology Conference* (IEEE, Piscataway, NY) **233, 1998**
12. J.M. Paik, K.C. Park, and Y.C. Joo, *J. Elec. Matls*. **33**, No. 1, p. 48, **2004**

13. S. P. Baker, Y. C. Joo, M. P. Knaub, and E. Artz, "Electromigration Damage in Mechanically Deformed Al Conductor Lines: Dislocations as Fast Diffusion Paths," *Acta mater*. **48**, p. 2199, **2000**
14. H. J. Frost and M. F. Ashby, *Deformation-Mechanism Maps: The Plasticity and Creep of Metals and Ceramics*. Pergamon Press, Oxford, p. 21, **1982**
15. D. Gan, P. S. Ho, Y. Pang, R. Huang, J. Leu, J. Maiz, and T. Scherban, "Effect of Passivation on Stress Relaxation in Electroplated Copper Films," *J. Mater. Res*. **21**, No. 6, p. 1512, **2006**
16. B. Cai, Q. P. Kong, L. Lu and K. Lu, "Interface Controlled Diffusional Creep of Nanocrystalline Pure Copper," *Scripta Mat.* **41**, p. 755, **1999**
17. W. Dickenscheid, R. Birringer, H. Gleiter, O. Kanert, B. Michel and B. Gunther, *Sol. Stat. Commun.* **79**, p. 683, **1991**
18. Z. Suo, "Electromigration-induced Dislocation Climb and Multiplication in Conducting Lines," *Acta Metall. Mater*. **42**, p. 3581, **1994**
19. A. S. Oates, "Electromigration Transport Mechanisms in Al Thin-film Conductors," *J. Appl. Phys*. **79**, p. 163, **1996**
20. J. R. Black, *6th Annual IEEE Intl. Rel. Phys. Symp. Proc.,* p. 148, **1967**
21. M. Shatzkes and J. R. Lloyd, *J. Appl. Phys*. **59**, p. 3890, **1986**
22. K. A. Danso and L. Tullos, *Microelectronic Reliability* **21**, p. 513, **1981**
23. H. A. Schafft, T. C. Grant, A. N. Saxena and C. Y. Kao, *23rd Annual IEEE Intl. Rel. Phys. Symp. Proc.,* p. 93, **1985**
24. R. Kirchheim and U. Kaeber, "Atomistic and Computer Modeling of Metallization Failure of Integrated Circuits by Electromigration," *J. Appl. Phys*. **70**, p. 172, **1991**

25. A. S. Budiman, C. S. Hau-Riege, P. R. Besser, A. Marathe, Y. -C. Joo, N. Tamura, J. R. Patel, and W. D. Nix., *45th Annual IEEE Intl. Rel. Phys. Symp. Proc.,* p. 122-127, **2007**

26. A. S. Budiman, C. S. Hau-Riege, P. R. Besser, A. Marathe, Y. -C. Joo, N. Tamura, J. R. Patel, and W. D. Nix., *9th International Workshop on Stress-induced Phenomena in Metallization AIP Proc.* **945**, p. 56, **2007**

27. E. Zschech, M. A. Meyer, and E. Langer, "Effect of Mass Transport Along Interfaces and Grain Boundaries on Copper Interconnect Degradation," *Mat. Res. Soc. Proc.* **812**, F.7.5.1, **2004**

APPENDIX

The parameter D_{core} takes into consideration only the diffusion along the dislocation cores for the overall length of specimen of interest, which would be true only for a single crystal Cu along the full length of the line. In this study, the lines are polycrystalline, and thus the effect of grain boundary diffusion must be considered. Here we study quantitatively the impact of grain boundary diffusivity on the overall dislocation core diffusion ($D_{core}^{effective}$).

We first consider the grain boundary region as illustrated in Figure 13, and suggest a relation between the mean distance, R, that atoms need to travel in the grain boundary region before finding another set of dislocation cores belonging to the next grain, and the dislocation density, ρ_{core}, in the Cu lines induced by the electromigration process itself. As can be expected, R is inversely related to ρ_{core} (or in other words, the more dislocation cores in the cross-section of the Cu lines, the smaller the diffusion distance in the grain boundary region).

We can deduce that, based on the illustration in Figure 13, that

$$R = \frac{l}{\sqrt{2}}; \rho_{core} = \frac{1}{l^2},$$

and thus,

$$R = \frac{1}{\sqrt{2\rho_{core}}} \quad . \qquad \text{(Eq. 6)}$$

where l is the mean distance between dislocation cores, and R is the mean distance of grain boundary diffusion. We can now consider the effective diffusion along a hypothetically continuous dislocation core, as well as the actual diffusion along the dislocation core and along the grain boundaries connecting dislocation cores in one grain with those in another, for a grain size, L. For the effective core diffusion along the hypothetical dislocation core of length L, the flux, J_{eff}, can be expressed as

$$J_{eff} = -\frac{D_{core}^{eff} c}{kT} \frac{d\mu}{dx} \quad , \qquad \text{(Eq. 7)}$$

where $c = 1/\Omega$ (c = concentration of diffusing species; Ω = atomic volume), μ = chemical potential, x is the axis of the diffusion direction along the dislocation core, and D_{core}^{eff}, k and T have been defined before. This is illustrated in Figure 14(a).

We now consider the combined diffusion along the actual dislocation cores (D_{core}) and along the adjoining grain boundary (D_{gb}), for a normalized diffusion distance, L. The D_{core}^{eff} is simply the dislocation core diffusivity when grain boundary diffusion for a mean distance, R, has been considered. This is again illustrated in Figure 14(b). The δ_{gb} is the effective width of the grain boundary.

The mass flow along a dislocation core, q_{core}, is simply

$$q_{core} = J_{eff} a_{core} \ , \qquad \text{(Eq. 8)}$$

as is clear from Figure 14(a), where a_{core} is the cross-sectional area of a dislocation core ($= \pi r_{core}^2$). The mass flows in Figure 14(b) consist of:

1) mass flow along the dislocation core, q_{core}
2) mass flow along the grain boundary region, q_{gb}

Now considering the diffusion along a dislocation core of length, L, as driven by the chemical potential difference, $\Delta\mu_1$, it is expected that

$$J_1 = -\frac{D_{core}}{kT\Omega} \frac{\Delta\mu_1}{L} \ , \qquad \text{(Eq. 9)}$$

which leads to

$$q_{core} = J_1 a_{core} = \left(-\frac{D_{core}}{kT\Omega} \frac{\Delta\mu_1}{L}\right)(\pi r_{core}^2) \ . \qquad \text{(Eq. 10)}$$

Along the grain boundary region, which can be modeled as a donut-shaped disc (Figure 15) with disc thickness, δ_{gb}, and inner diameter, r_{core}, and outer diameter, R, the diffusion can be described as follow

$$q_{gb} = J_2 (2\pi r \delta_{gb}) \ , \qquad \text{(Eq. 11)}$$

or equivalently,

$$q_{gb} = 2\pi r \delta_{gb} \left\{ -\left(\frac{D_{gb}}{kT\Omega} \right) \frac{d\mu}{dr} \right\} \ , \qquad \text{(Eq. 12)}$$

where q_{gb} is the mass flow along the grain boundary, and J_2 is the grain boundary mass flow per area, while the variables μ and r are the chemical potential and radius/distance of diffusion from the center of the disc, respectively. However q_{gb} is not a function of r ($\neq f(r)$), and thus should be a constant. Consequently, by rearranging Equation 12, we find

$$-q_{gb}\frac{kT\Omega}{2\pi\delta_{gb}D_{gb}}=\frac{d\mu}{dr}=const. \qquad \text{(Eq. **13**)}$$

Integrating and further rearranging leads to

$$\Delta\mu_2=-q_{gb}\frac{kT\Omega}{2\pi\delta_{gb}D_{gb}}\ln\left(\frac{R}{r_{core}}\right), \qquad \text{(Eq. **14**)}$$

where $\Delta\mu_2$ is simply the integrated chemical potential difference for diffusion along the grain boundary region from $r = r_{core}$ to $r = R$.

In the combined diffusion along the actual dislocation core and along the grain boundary region (Figure 14(b)), mass conservation requires

$$q_{core}=q_{gb}, \qquad \text{(Eq. **15**)}$$

which after substituting Equations 10 and 14 would lead to

$$-\pi r_{core}^2\frac{D_{core}}{kT\Omega}\frac{\Delta\mu_1}{L}=-\Delta\mu_2\frac{2\mu\delta_{gb}D_{gb}}{kT\Omega\ln(R/r_{core})}. \qquad \text{(Eq. **16**)}$$

Obviously, the combined chemical potential, $\Delta\mu$, can be described as follows

$$\Delta\mu=\Delta\mu_1+\Delta\mu_2. \qquad \text{(Eq. **17**)}$$

Combining Equations 16 and 17, we find

$$\Delta\mu_1 = \left\{ \frac{2\delta_{gb} D_{gb} L}{2\delta_{gb} D_{gb} L + r_{core}^2 D_{core} \ln(R/r_{core})} \right\} \Delta\mu \ . \qquad \text{(Eq. } \mathbf{18}\text{)}$$

To derive the effective diffusivity of the core diffusion, D_{core}^{eff}, we rewrite Equation 10

$$q_{core} = -\pi r_{core}^2 \frac{D_{core}}{kT\Omega} \frac{\Delta\mu_1}{L} \ ,$$

and by substituting Equation 18, we find

$$q_{core} = -\pi r_{core}^2 \frac{D_{core}}{kT\Omega} \left\{ \frac{2\delta_{gb} D_{gb} L}{2\delta_{gb} D_{gb} L + r_{core}^2 D_{core} \ln(R/r_{core})} \right\} \frac{\Delta\mu}{L}, \qquad \text{(Eq. } \mathbf{19}\text{)}$$

which suggests that

$$D_{core}^{eff} = D_{core} \left\{ \frac{2\delta_{gb} D_{gb} L}{2\delta_{gb} D_{gb} L + r_{core}^2 D_{core} \ln(R/r_{core})} \right\}. \qquad \text{(Eq. } \mathbf{20}\text{)}$$

FIGURE CAPTIONS

FIG. 1. SEM images and schematic drawings of the Cu interconnect test structures in this experiment; (a) SEM image of the test structure; (b) *in situ* electromigration experiment; (c) two sets of test structures of different dielectric schemes: low-*k* vs hybrid.

FIG. 2. The typical evolution of Laue diffractions spots from Cu interconnect test structures during *in situ* electromigration experiments.

FIG. 3. Laue diffraction images of the cathode end of the line after 36 hours of testing. In the images at left (a), streaking and/or splitting of Cu Laue diffractions spots throughout a segment of the line is observed. Dislocations were observed with cores aligned with the direction of the electron flow in the line (consistent with earlier observations[4-6]) across grains throughout the length of the segment of the line are observed, as shown schematically at right (b) (*Grain map is estimated based on streaking observation).

FIG. 4. Dielectric effects: the Laue peak streaking/splitting observed from Cu interconnect test structures with (a) low-*k*, and (b) hybrid dielectrics; in χ-θ space/contour intensity plot.

FIG. 5. Samples A vs. B comparison: the schematic of the cross-sections (color code refers to different materials), typical evolution of Cu Laue diffraction spots (from "Initial" to "EM" states), and lastly, the typical densities of GNDs implied by the extent of streaking/splitting of Laue peaks; (a) Samples A (Cu lines reported in our previous studies[4-6]); and (b) Samples B (Cu

lines reported in this study); They were fabricated by different manufacturers. (*Taken as that of typical annealed metals)

FIG. 6. Comparison of Samples A vs. B: the texture correlation; (a) Samples A (from References 4-6) have a weak (111) texture, and "less plasticity," whereas; (b) Samples B (Cu lines reported in this study) have strong (111) texture, and "more plasticity." The schematic at right illustrates that the strong preferred in-plane orientation of (111) grains leads to a preferred <110> to the sidewalls and <112> along the direction of length of the lines (Courtesy of Besser *et al.*[10]).

FIG. 7. Schematic of a grain containing same-sign edge dislocations with cores running along the direction of the electron flow in the interconnect line.

FIG. 8. Illustration of bamboo grains with dislocation cores running along the direction of the electron flow in the line under electromigration bias. Dislocation cores from one grain end at the grain boundaries. Atoms traveling across multiple grains must diffuse along grain boundary regions, before finding another set of dislocation cores in the next grain.

FIG. 9. Comparison of diffusivities as a function of temperature between D_{core} (only dislocation core diffusion, no grain boundary), D_{core}^{eff} (considering the effect of grain boundary; as it is – as shown in Table 2), and an extreme D_{core}^{eff} (considering the effect of grain boundary diffusion as if it is lattice diffusion). Diffusivities were calculated using values summarized in Table 1.

FIG. 10. Calculated diffusivities as a function of temperature between the interface diffusion path and those of dislocation cores of various densities in Cu interconnect lines ($10^{12}/m^2$, $10^{15}/m^2$, $10^{17}/m^2$). Each diffusion mechanism is assumed to act alone.

FIG. 11. Kirchheim and Kaeber's experimental *MTF* data[24] (reproduced manually here to the highest accuracy possible from Reference 24; for clarity and improved image resolution) as a function of reduced current density, $j - j_{crit}$ (all the solid features); The dotted and dashed lines are added to lead to our argument.

FIG. 12. Illustration of the impact of the current exponent (n) on the extrapolated lifetime. The danger of overestimation of device lifetime by using $n > 1$ is shown (dotted-dashed line), as is the more conservative extrapolation using $n = 1$ (dashed line), which is closer to the actual device lifetime in use conditions. The reproduced Kirchheim and Kaeber's experimental *MTF* data[24] is again used here for illustrative purposes.

FIG. 13. Illustration of the grain boundary region of two bamboo grains with dislocation cores running along the direction of the electron flow in the line under an electromigration bias. Atoms traveling along the cores of the first grain (solid lines, closed circles) must diffuse in grain boundary regions for the distance, R, before finding another set of dislocation cores in the next grains (dashed lines, open circles).

FIG. 14. Illustration of (a) a hypothetically continuous dislocation core diffusion along a specified diffusion distance, L, and (b) the combined effects of dislocation cores and grain

boundaries along a normalized diffusion distance where δ_{gb} is the effective width of the grain boundary.

FIG. 15. Illustration of the diffusion along the grain boundary region with indications of the parameters (R, r_{core}, q_{gb} and δ_{gb}) as used in the analyses.

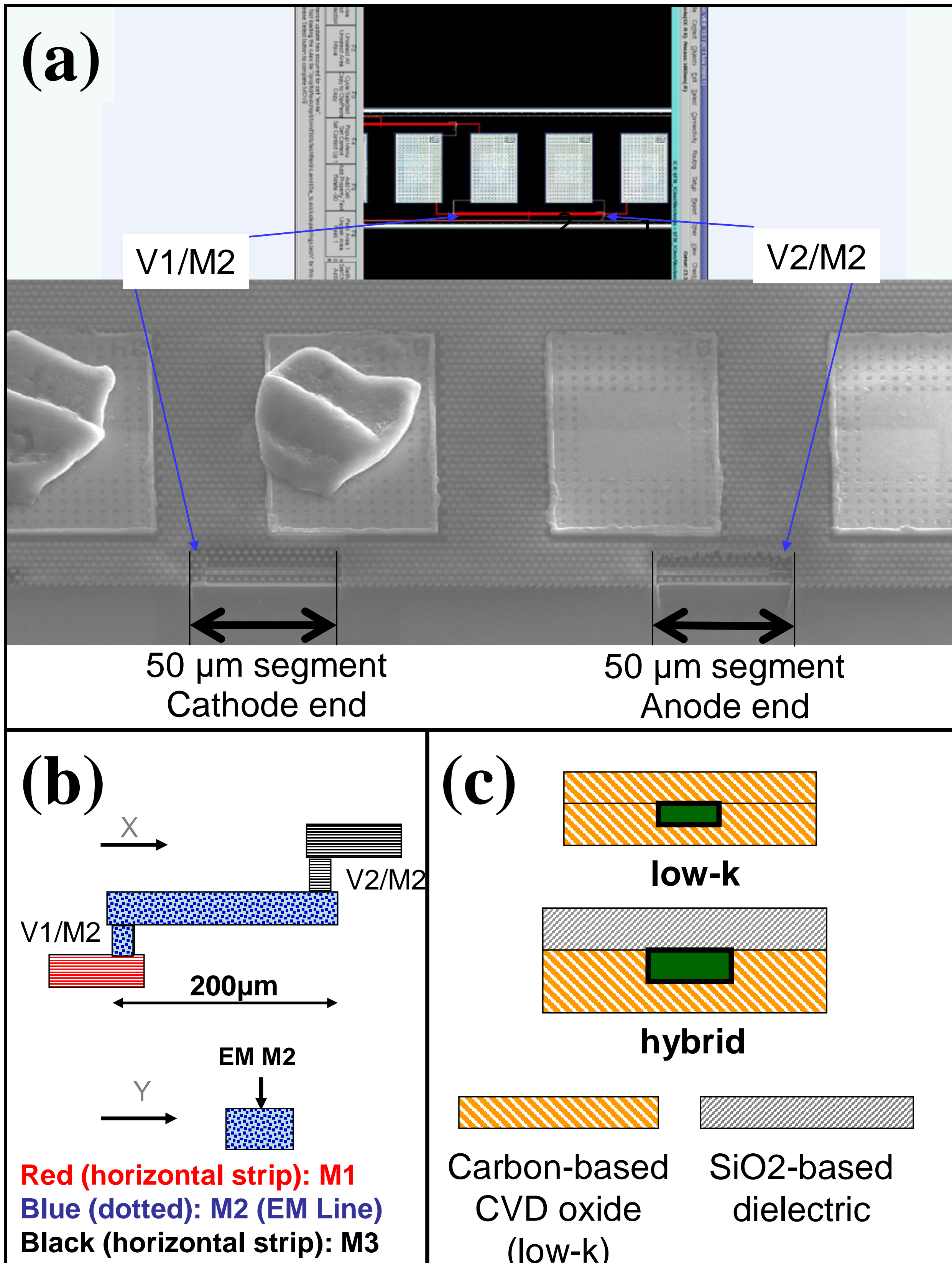

Figure 1

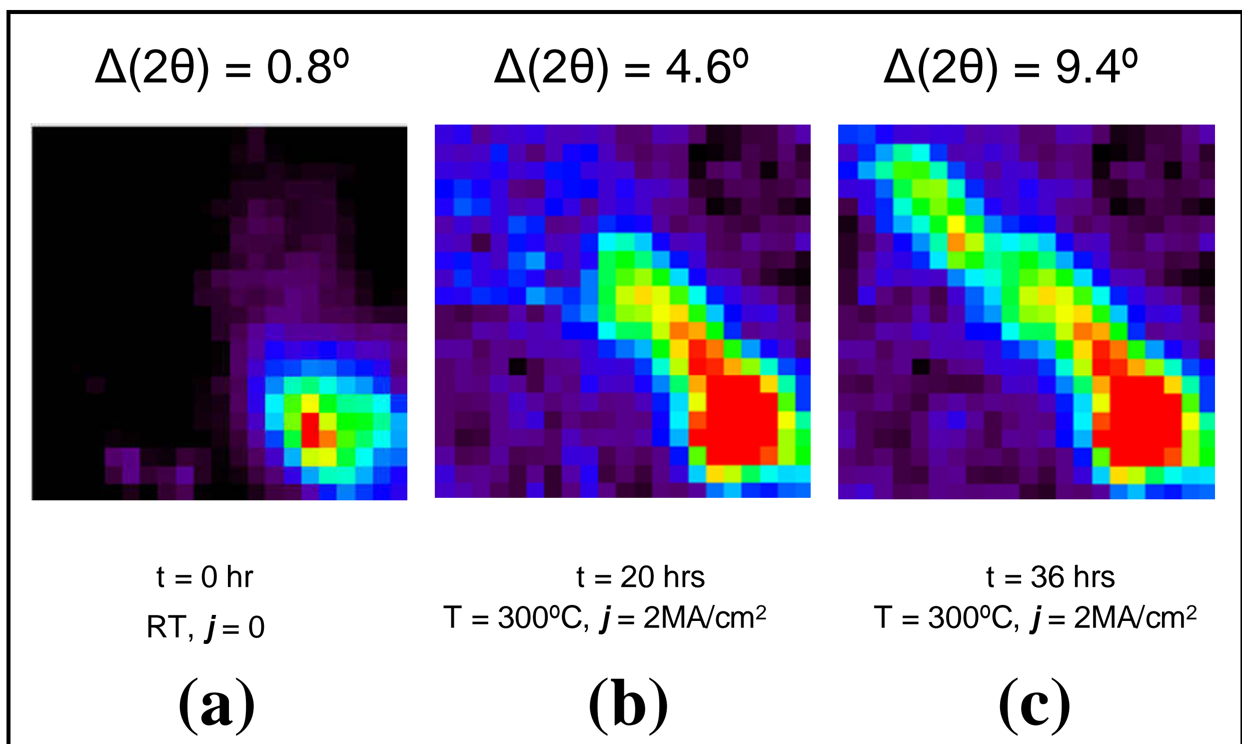

Figure 2

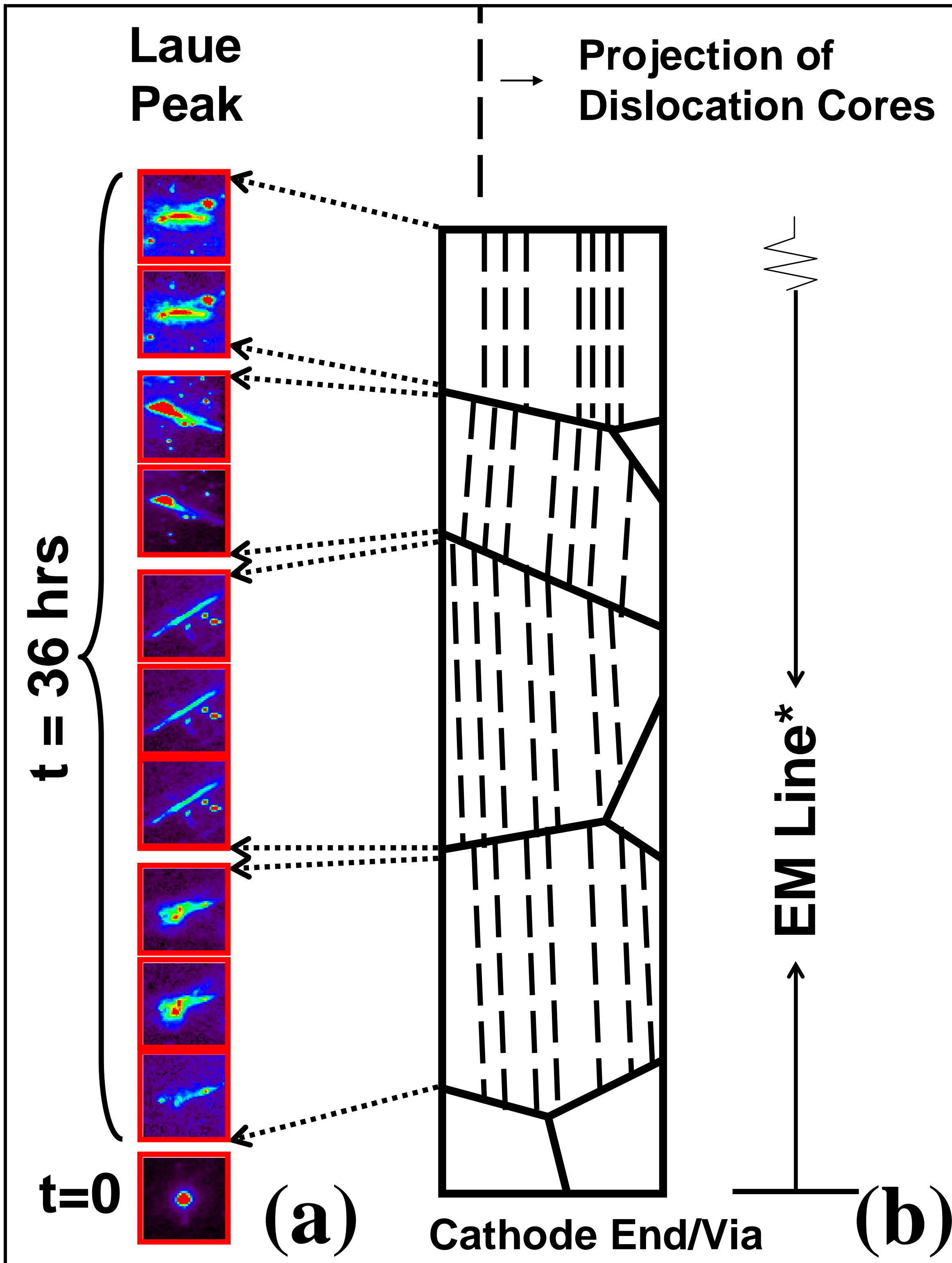

Figure 3

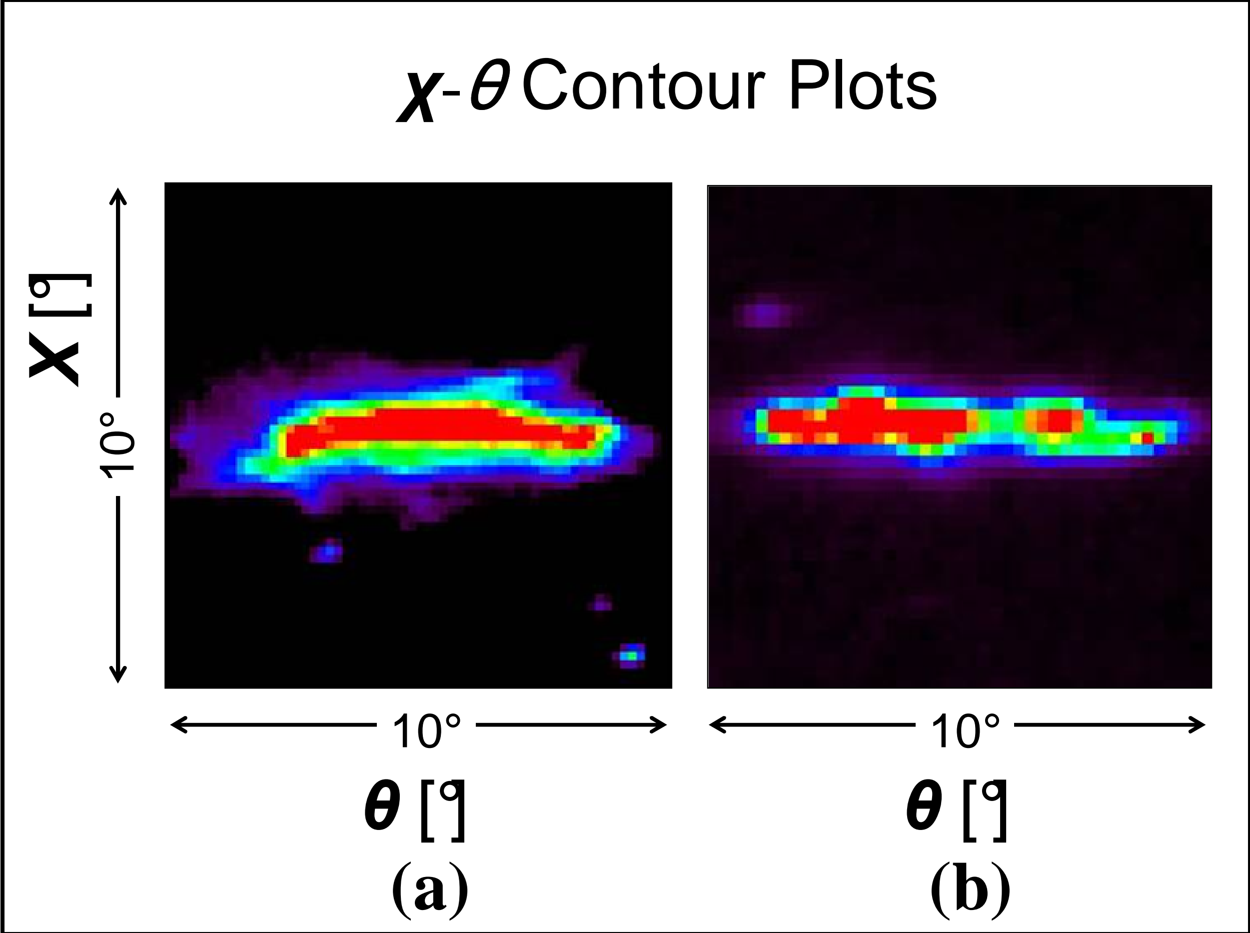

Figure 4

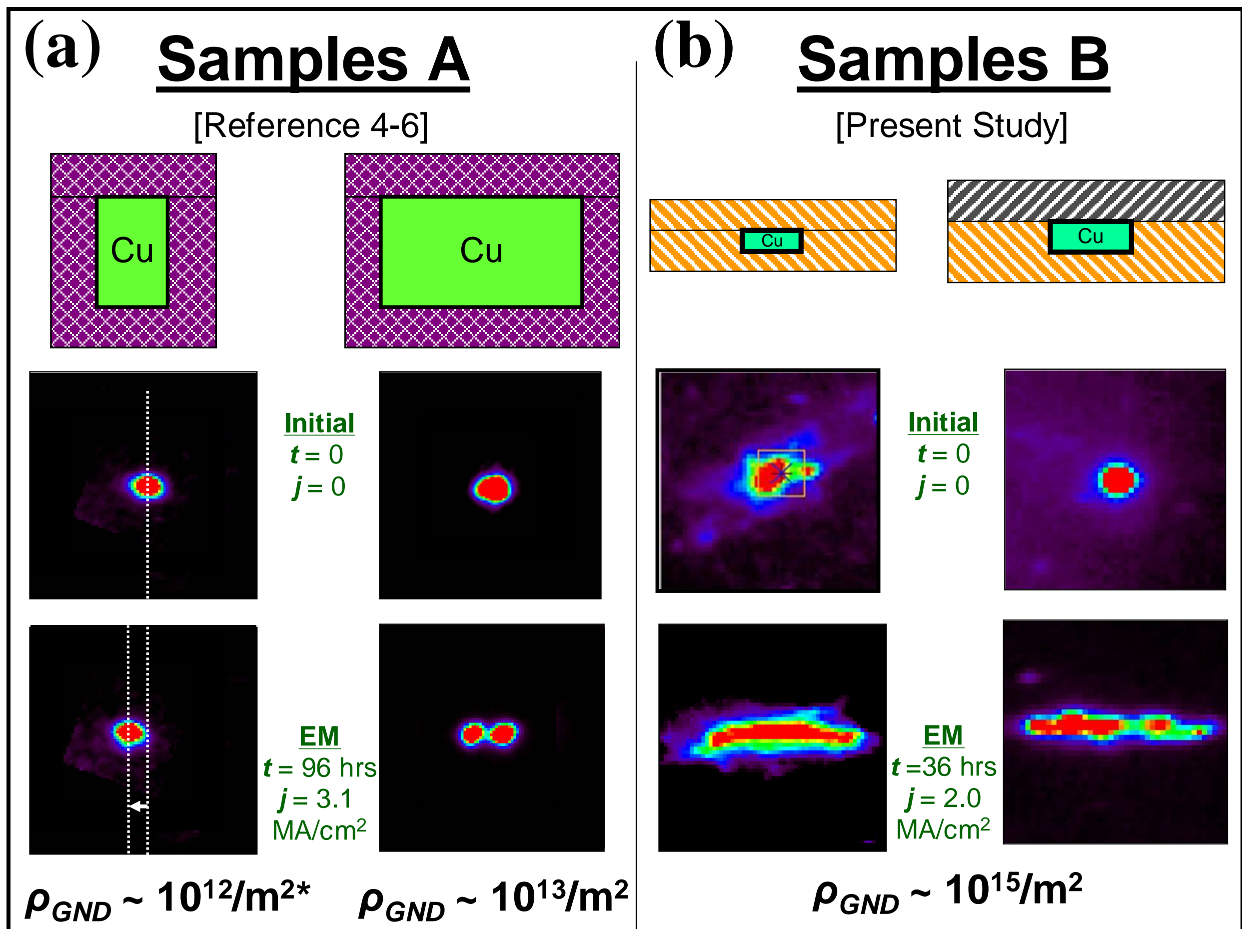

Figure 5

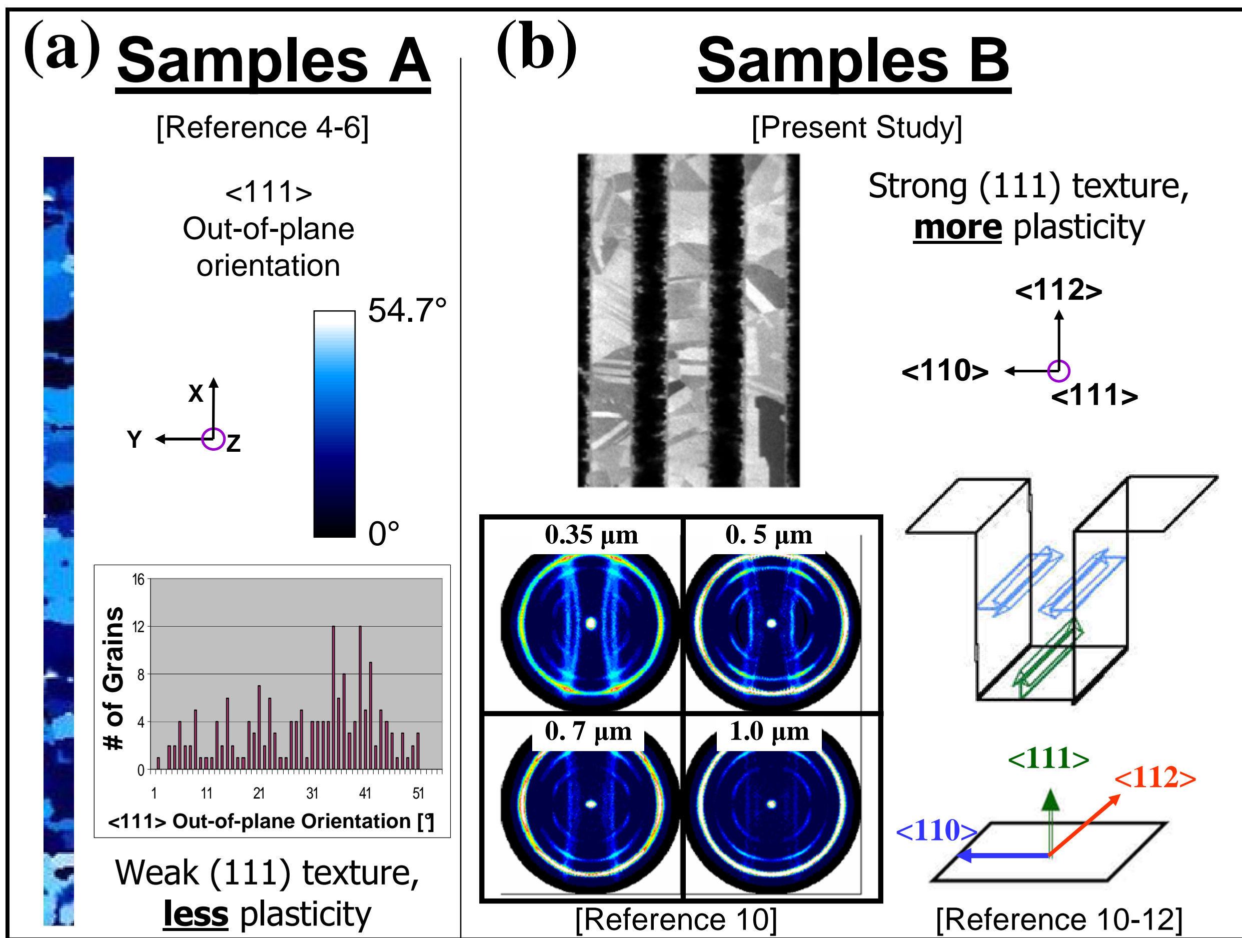

Figure 6

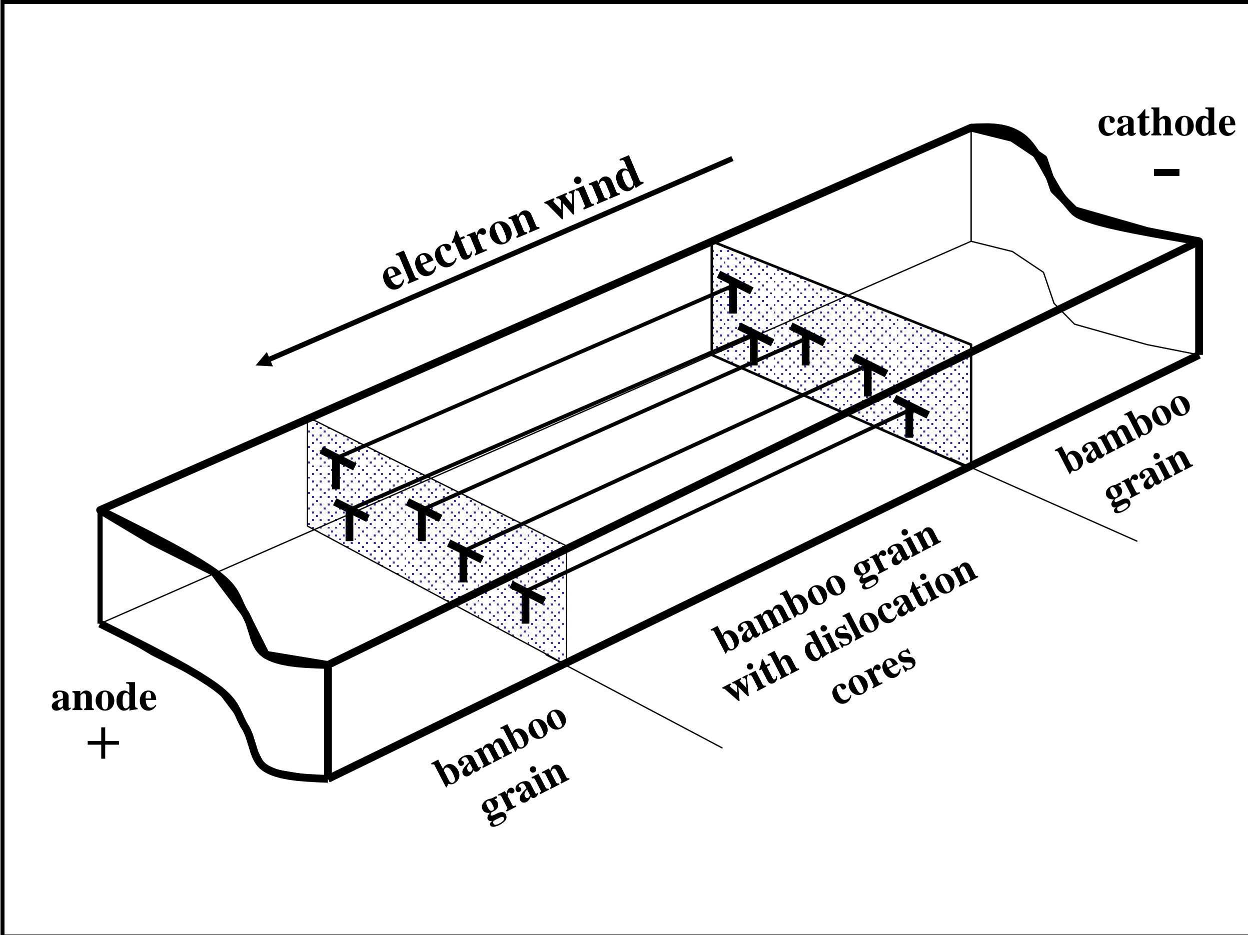

Figure 7

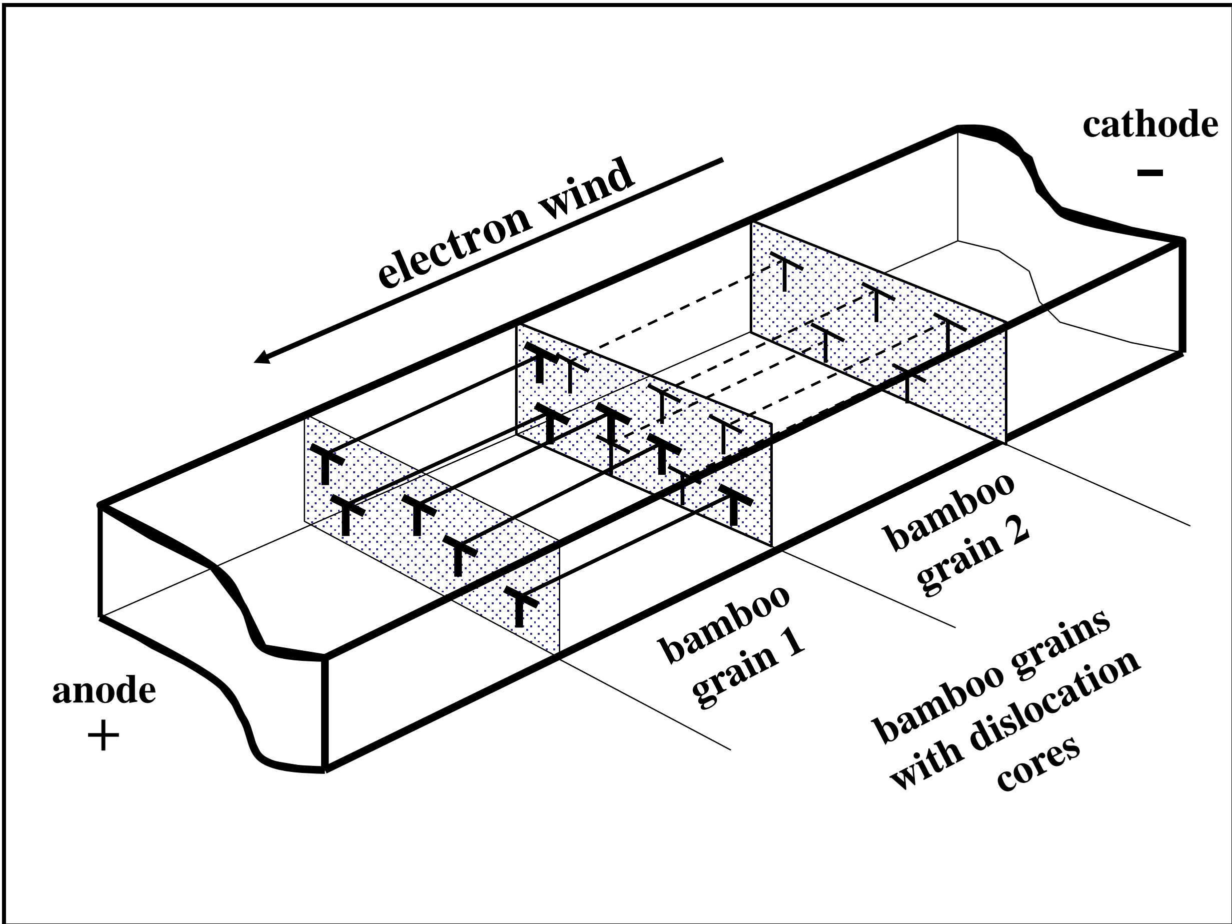

Figure 8

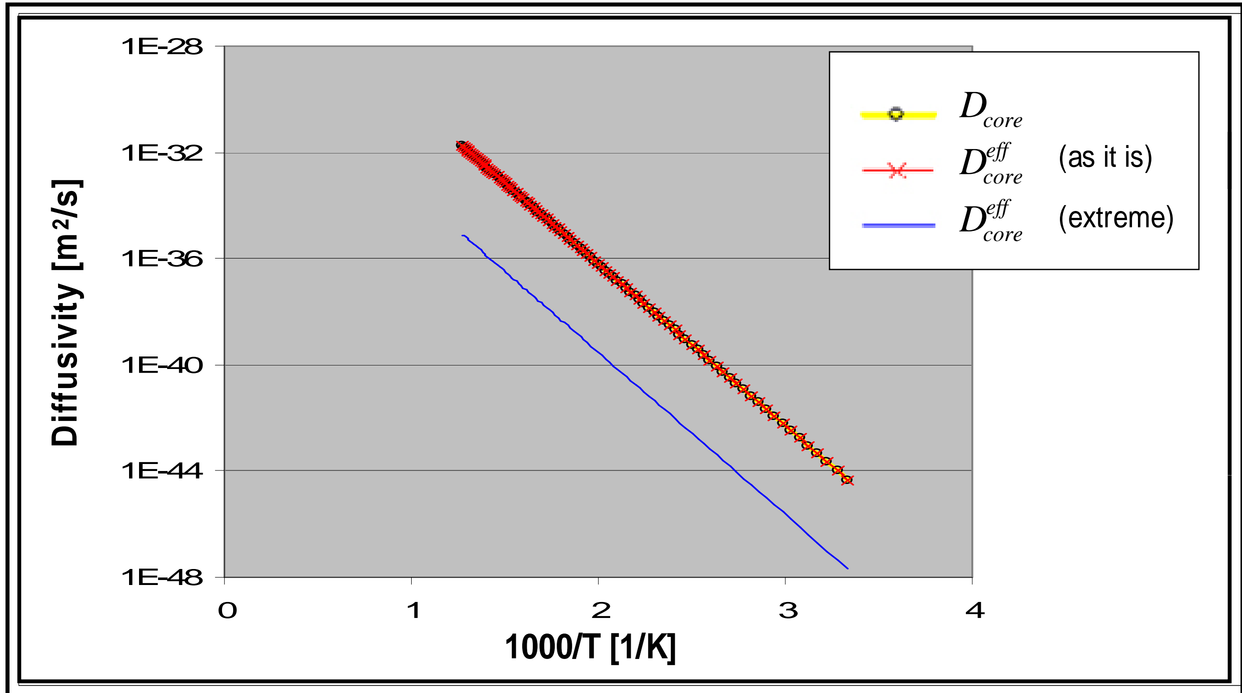

Figure 9

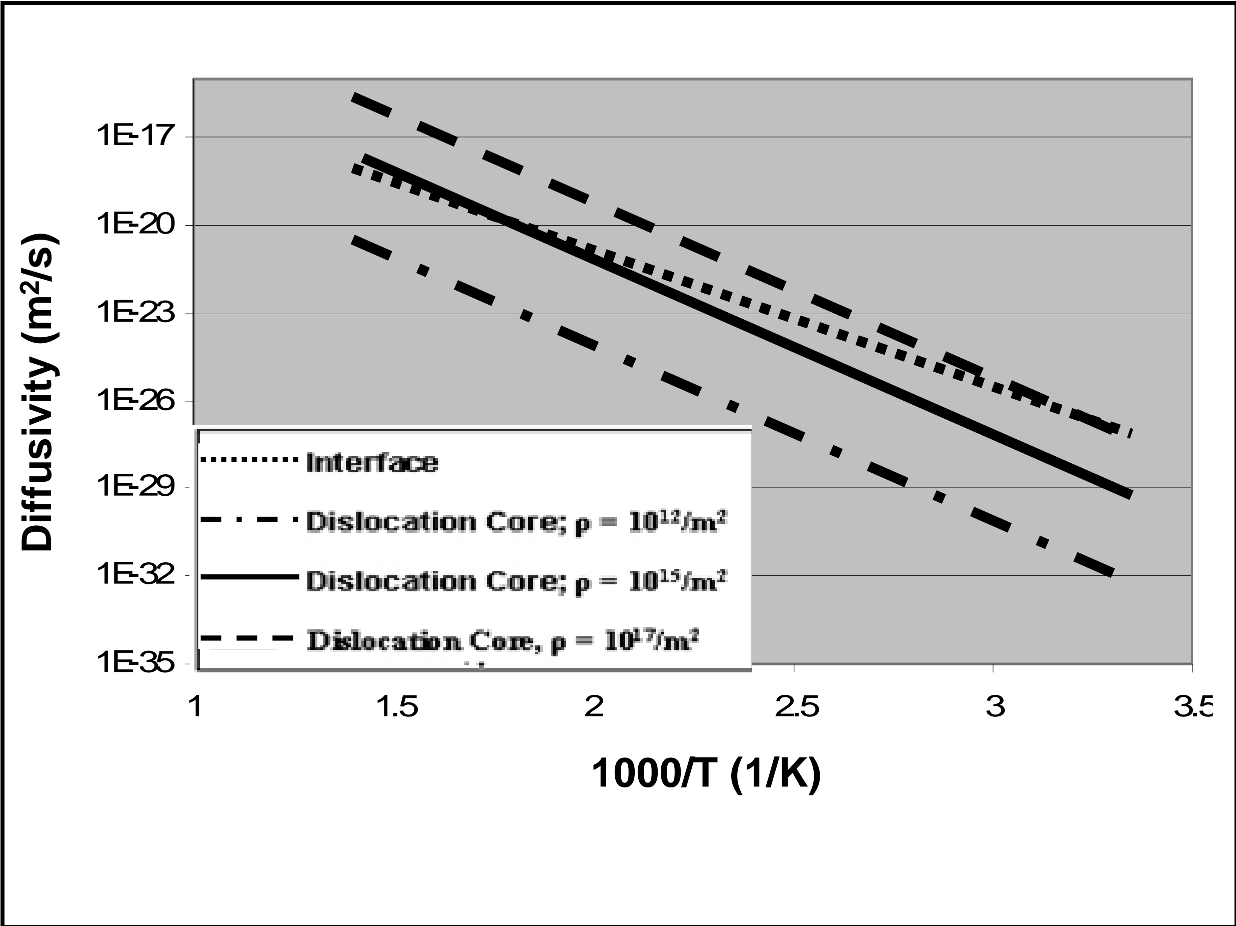

Figure 10

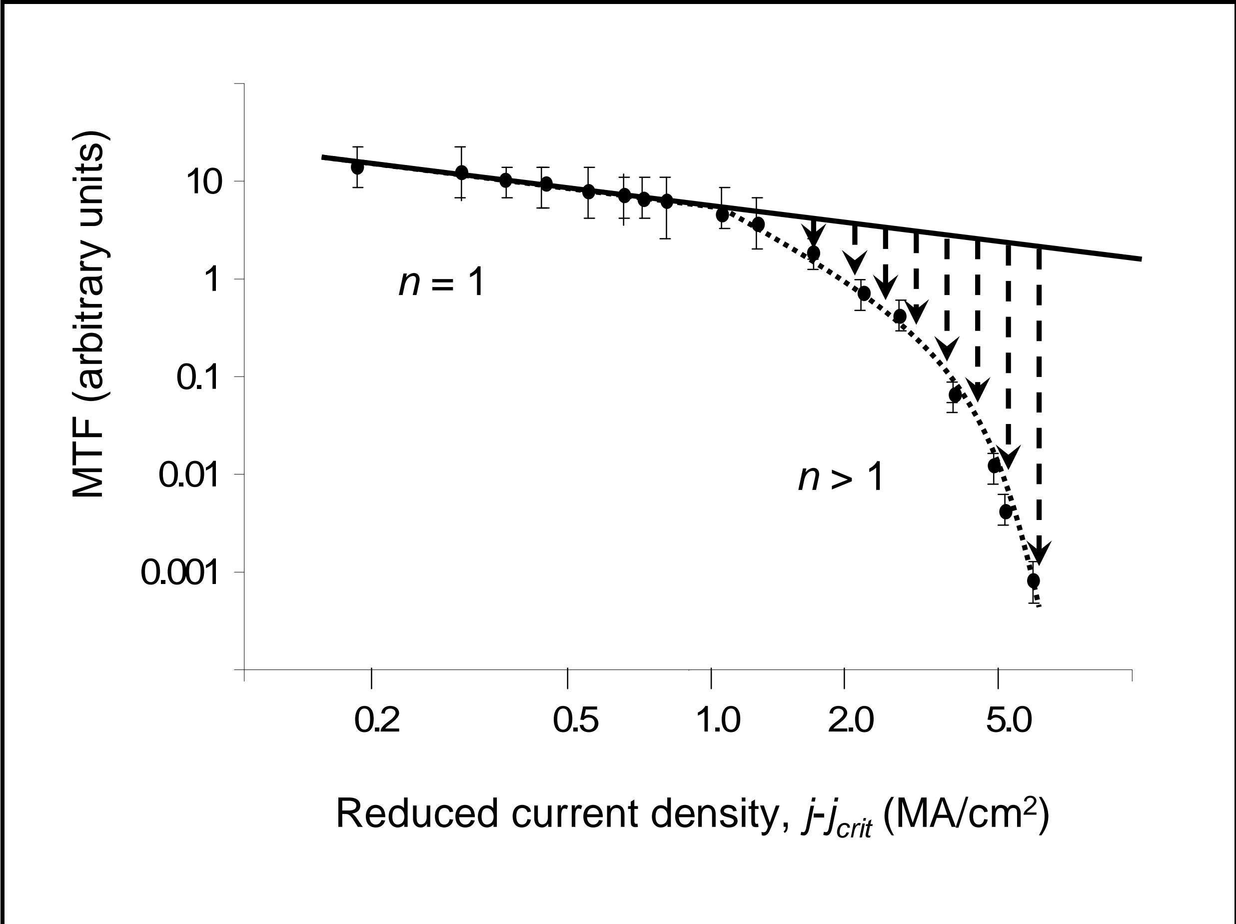

Figure 11

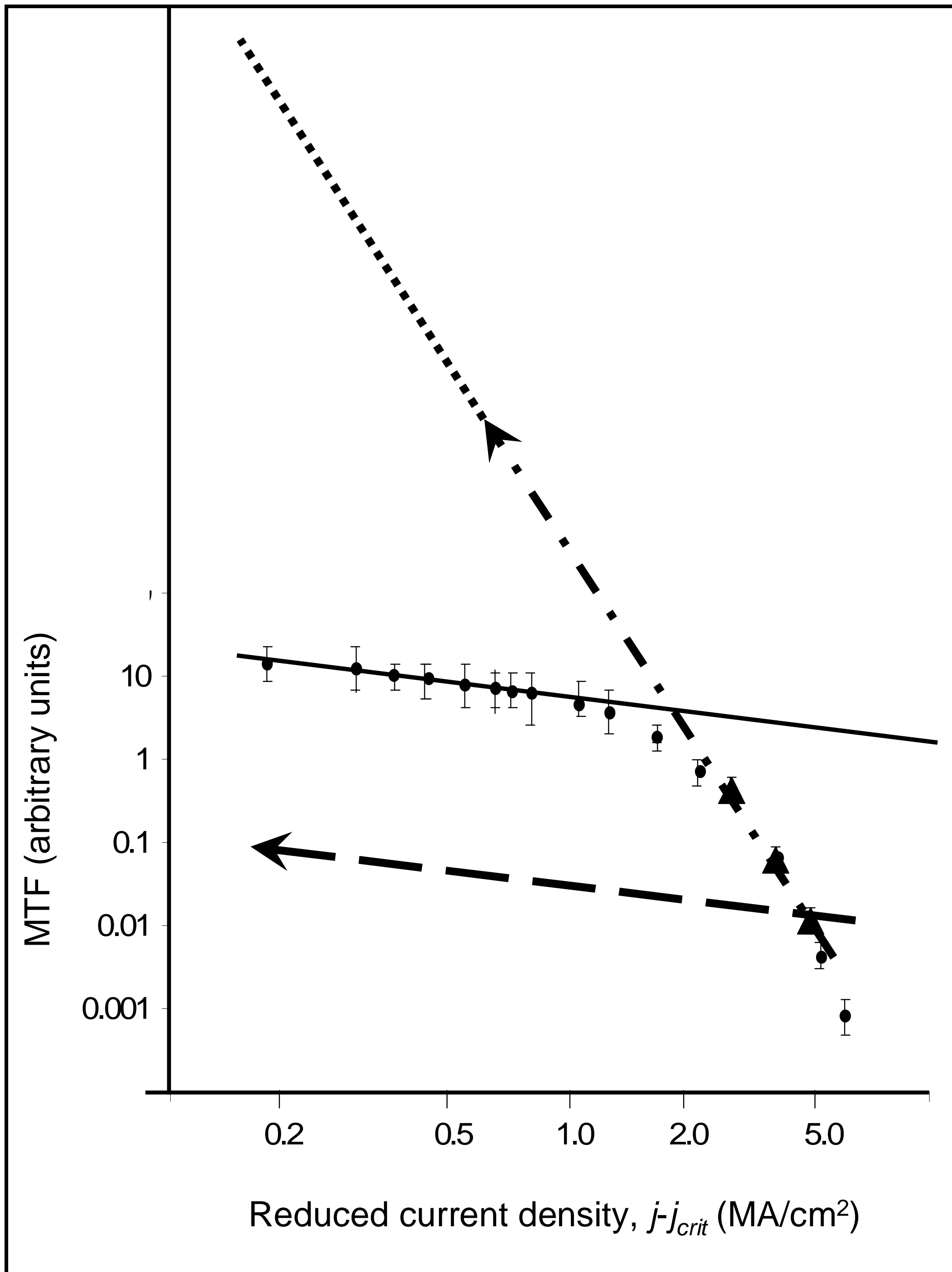

Figure 12

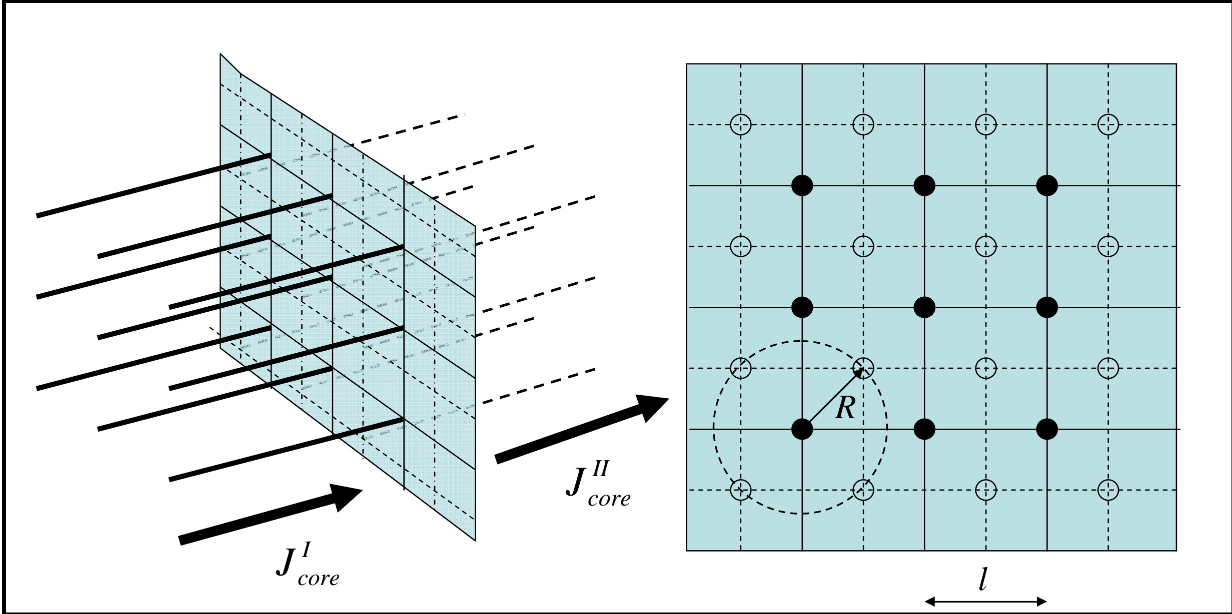

Figure 13

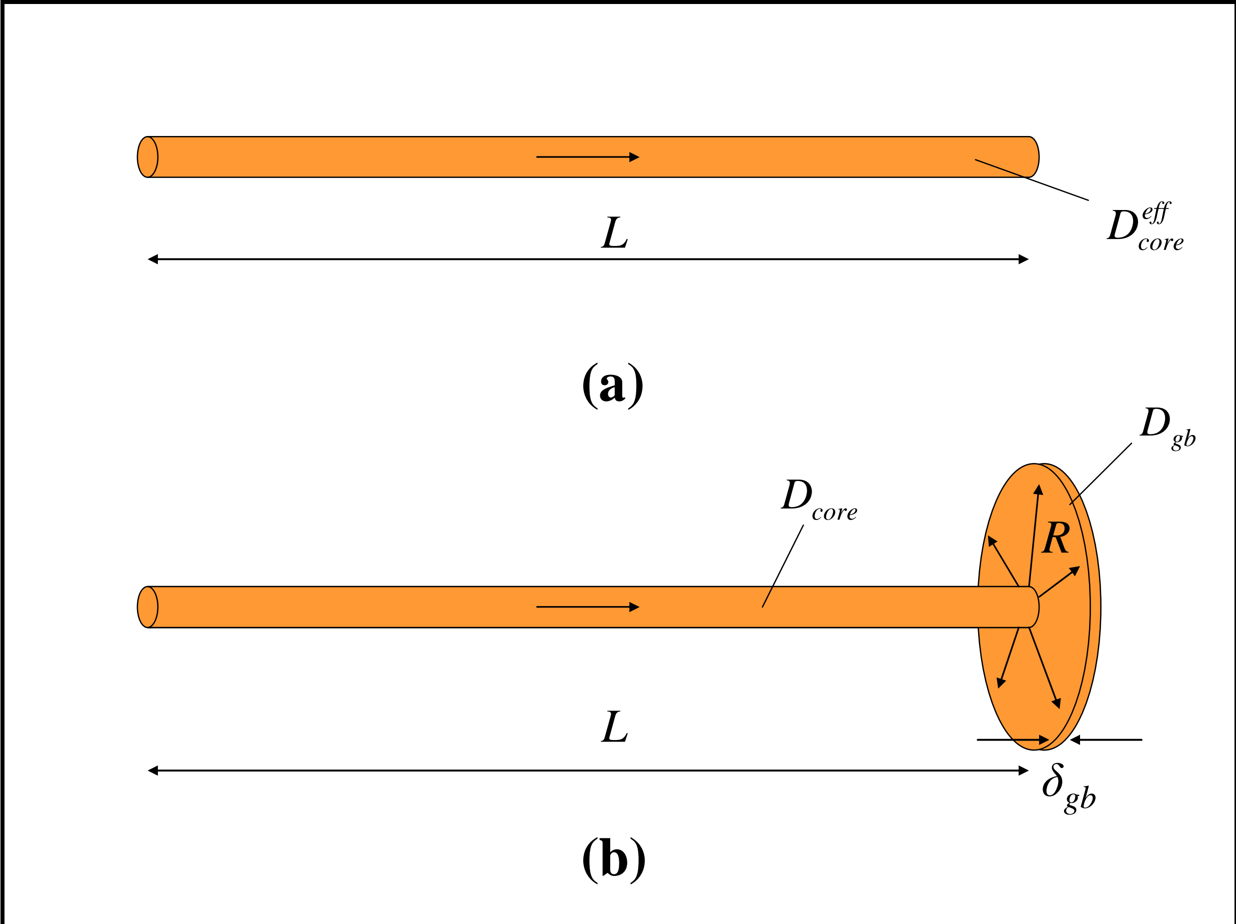

Figure 14

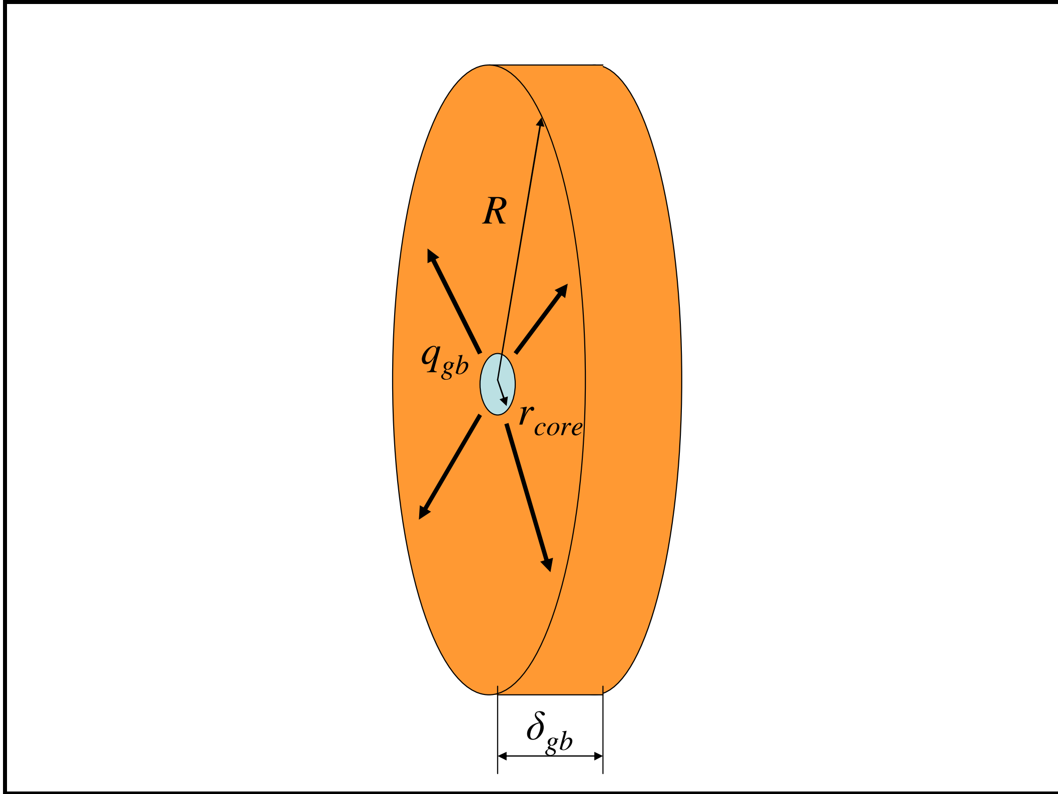

Figure 15

TABLE CAPTIONS

TABLE 1. Values used to determine influence of grain boundary diffusion on the overall transport kinetics in the Cu line under EM. The diffusivities (D_{gb}, D_{core}) are described in the usual way by $D = D_o \exp(-E_A/kT)$ where E_A is the activation energy, D_o is the pre-exponential constant, and k is the Boltzmann's constant. The subscripts *gb* refers to grain boundary diffusion.

TABLE 2. Values of the two parameters/terms in Equation 3 (or denominator of Equation 2) calculated based on values listed in Table 1.

TABLE 3. Values used to determine diffusions in Cu interconnects as a function of temperature (Figure 10). D_o is the pre-exponential constant and E_A is the activation energy. The subscripts *int* and *core* refer to interface and core diffusions, respectively. The δ is the effective interface diffusion thickness, h is the thickness of the Cu lines, and a_{core} is the area of a dislocation core.

Variable	Value	Reference/Remarks
T	300° C = 573 K	Following T_{test} in "Experimental"
$E_{A,gb}$	1.08 eV	Refs. 14-17
$\delta_{gb}D_{gb}$	1.6×10^{-24} m^3/s	Calculated, Ref. 14
L	1 µm	Estimated based on "Results"
r_{core}	0.25Å	Ref. 14
$E_{A,core}$	1.21 eV	Ref. 14
$r_{core}^2 D_{core}$	7.3×10^{-36} m^4/s	Calculated, Ref. 14
ρ_{GND}	10^{15}/m^2	As observed in "Results"
R	22 nm	$R = 1/2\rho_{core}$

Table 1

Parameter/Term in Equation 17	**Value**
$2\delta_{gb}D_{gb}L$	3.2 x 10^{-30} m^4/s
$r_{core}^2 D_{core} \ln(R/r_{core})$	5.0 x 10^{-35} m^4/s

Table 2

Variable	Value	Reference/Remarks
$\delta D_{o,int}$	3.4 x 10^{-19} m^3/s	Based on SiN/Cu, Ref. 15
h	0.2 μm	"Experimental" Section
$E_{A,int}$	0.91 eV	Based on SiN/Cu, Ref. 15
$a_{core}D_{o,core}$	1.0 x 10^{-24} m^4/s	For copper, Ref. 14
$E_{A,core}$	1.21 eV	For copper, Ref. 14

Table 3